Dynamic Phasor Based Interface Model for EMT and Transient Stability Hybrid Simulations

Dewu Shu, *Student Member, IEEE*, Xiaorong Xie, *Senior Member, IEEE*, Venkata Dinavahi, *Senior Member, IEEE*, Chunpeng Zhang, *Member, IEEE*, Xiaohui Ye, and Qirong Jiang, *Member, IEEE*

***Abstract*—Electromagnetic transient (EMT) and transient stability hybrid simulations are predominantly used to analyze the interactions between HVDC systems and the ac grids. However, the dynamics of the converters will be greatly affected by the waveforms of adjacent ac systems. Waveform distortion as well as time delay caused by interfacing can significantly increase interface errors, resulting in the decrease of the overall accuracy of the simulations. To solve such problems, a dynamic phasor based interface model (DPIM) is proposed in this paper to improve the accuracy of interfaces, especially when the fault occurs near the converters. In doing so, the whole system is partitioned into three parts: the transient stability (TS) subsystem, the EMT subsystem, and the DPIM. During each iteration, the interfaces between the TS subsystem and DPIM are represented by their Norton equivalents at the fundamental frequency and Thevenin equivalents in the dynamic phasor form. Similarly, the interfaces between DPIM and EMT subsystems are represented by their three-phase Norton equivalents and Thevenin equivalents in dynamic phasors, respectively. The effectiveness concerning the accuracy and the efficiency of the proposed method is validated by simulating a practical HVDC Project.**

***Index Terms*—Dynamic phasors, electromagnetic transient (EMT), HVDC, hybrid simulation, interface model, transient stability.**

I. Introduction

LINE commutated converter (LCC) based HVDC system is often adopted for transmission of large-scale renewable energy, such as the Qinghai-Tibet HVDC project in China [1]–[4]. In order to analyze the interactions between HVDC and AC systems accurately and efficiently, the EMT and TS hybrid simulations is often used [5]–[9]. For hybrid simulations, the power system is first partitioned into one TS subsystem, different EMT subsystems and the interface model according to different levels of detail. And the interface model is used to reflect the interactions between them. The hybrid simulations can satisfy both the accuracy requirements of detailed power electronic devices and the efficiency requirements of large-scale power systems, as the power grids are simulated with a large time-step TS program and local detailed power electronic systems are simulated with small time-step EMT programs.

Previous studies of hybrid simulations mainly focused on improving the accuracy of the interface model as well as the overall efficiency [6]–[11]. Particularly, the waveforms of adjacent AC systems have a great impact on the dynamic characteristics of the HVDC converter, especially if the effective short circuit ratio (ESCR) is lower than 2.5. When the fault nears the interface bus of the converter, the decreased accuracy of the interface model will reduce the overall simulation accuracy greatly. Moreover, one interaction step delay exist for the calculations of parameters of the interface model. Therefore, developing the interface model is the key to improving the overall simulation accuracy of the hybrid simulations. Norton/Thevenin equivalents in the time-domain are generally adopted as the interface model between TS and EMT subsystems, where the interface line is represented as the PI-section branch [6], [7]. In [6], the influence of frequency on the parameters of interfaces are taken into account to improve the accuracy of interfaces in the EMT subsystems. One method to improve the accuracy of the interface model in the EMT subsystem is the frequency dependent network equivalent (FDNE) method [8], [9]. However, its drawback lies in the relatively low computational efficiency and spurious transients during a switching operation of a new FDNE model. In [11], the waveform distortion problems of EMT subsystems are mitigated by extending the interface buses far into the AC grids in order to comply with the three-phase balanced assumption. However, the simulation accuracy of this method is still unsatisfactory and the efficiency was severely curtailed. When the fault occurs near the converter, it is very important to improve the accuracy of the interface model in the TS subsystem, i.e., the Norton equivalents [12]. Typical techniques include the curve-fitting technique and the FFT/DFT technique [6], [8]. For the curve-fitting technique, data in multiple cycles are processed. Therefore, a large amount of computation affects the efficiency of this technique and the obtained parameters lack physical interpretations. Similarly, for the FFT/DFT technique, all the samples during the last cycle

Manuscript received March 9, 2017; revised August 8, 2017; accepted October 21, 2017. Date of publication October 25, 2017; date of current version June 18, 2018. This work was supported in part by the Major Program of the National Natural Science Foundation of China under Grant 51490683 and in part by the Research Project on Key Technologies and Demonstration Application of Flexible Coordinated Control of Electromagnetic Loop Network in Metropolitan Power Grid with High Load Density under Grant GZHKJ 00000101. Paper no. TPWRS-00342-2017. *(Corresponding author: Dewu Shu.)*

D. Shu, X. Xie, C. Zhang, X. Ye, and Q. Jiang are with the State Key Laboratory of Power System, Department of Electrical Engineering, Tsinghua University, Beijing 100084, China (e-mail: shudw13@mails.tsinghua.edu.cn; xiexr@tsinghua.edu.cn; zhangchunpeng@tsinghua.edu.cn; yexh15@mails.tsinghua.edu.cn; qrjiang@tsinghua.edu.cn).

V. Dinavahi is with the Department of Electrical and Computer Engineering, University of Alberta, Edmonton, AB T6G 2R3, Canada (e-mail: dinavahi@ualberta.ca).

Color versions of one or more of the figures in this paper are available online at http://ieeexplore.ieee.org.

Digital Object Identifier 10.1109/TPWRS.2017.2766269

should be calculated. The problems of the errors induced by the sampling delays and the large amount of computation still exist.

To resolve the above-mentioned problems, a novel dynamic phasor based interface model (DPIM) is proposed to improve the accuracy of interfaces when simulating large-scale AC/DC systems. The DPIM has the following important features:

1) The principle of DPIM is to use transmission lines as interfaces, by modeling their dynamic responses using dynamic phasors.
2) By using the dynamic phasors, the DPIM can improve the accuracy and reduce the computation of the interface model in the TS subsystem.
3) The interface model of the EMT subsystem, with its instantaneous values represented by dynamic phasors, can be efficiently updated with the proposed DPIM. Moreover, the errors caused by the sampling delays are effectively mitigated.

The rest of the paper is organized as follows: Section II demonstrates the proposed DPIM, including the mathematical model and its comparisons with the traditional method in accuracy and efficiency. In Section III, the proposed hybrid simulation method is illustrated, including its architecture, the interface models between TS/EMT subsystem and DPIM, and its overall computational scheme. Section IV verifies the effectiveness of the proposed method through the simulation of a practical HVDC system. Section V concludes this paper.

II. Proposed Interface Models

A. Dynamic Phasor Concept

The concept of dynamic phasor comes from the time-varying Fourier series. The signal $x(\tau)$, $\tau \in (t-T, t]$ with the period T is expressed in the form of time-varying Fourier series [13]–[15], i.e.,

$$\begin{cases} x(\tau) = \sum_{k=-\infty}^{\infty} \widehat{\boldsymbol{x}}_{\boldsymbol{k}}(t) e^{\mathrm{jk}\omega\tau}, \\ \widehat{\boldsymbol{x}}_{\boldsymbol{k}}(t) = \frac{1}{T}\int_{t-\tau}^{t} x(\tau) e^{-\mathrm{jk}\omega\tau} d\tau, \end{cases} \tag{1}$$

where $\omega = 2\pi/T$, $\widehat{\boldsymbol{x}}_{\boldsymbol{k}}(\boldsymbol{t})$ is the k^{th} dynamic phasor of $x(\tau)$. When the time window with the period of T moves along the time axes, the dynamic phasors are changed with the time t.

Two important features, i.e., the product feature and the differential feature of the dynamic phasor, are given as

$$\begin{cases} (\widehat{\boldsymbol{xy}})_{\boldsymbol{k}} = \sum_i \widehat{\boldsymbol{x}}_{\boldsymbol{k-i}} \widehat{\boldsymbol{y}}_{\boldsymbol{i}}, \\ \frac{d}{dt}\widehat{\boldsymbol{x}}_{\boldsymbol{k}} = \widehat{(\frac{d\boldsymbol{x}}{d\boldsymbol{t}})}_{\boldsymbol{k}} - jk\omega\widehat{\boldsymbol{x}}_{\boldsymbol{k}}. \end{cases} \tag{2}$$

Based on (1)–(2), the corresponding dynamic phasor models of power system components can be derived. For a component modelled with its algebraic differential equation

$$\begin{cases} \frac{dx}{dt} = Ax(t) + Bv(t), \\ i(t) = Cx(t) + Dv(t), \end{cases} \tag{3}$$

where x represents state variables; $v(t), i(t)$ refer to the voltage and the current of the component; A, B, C, D are the parameters.

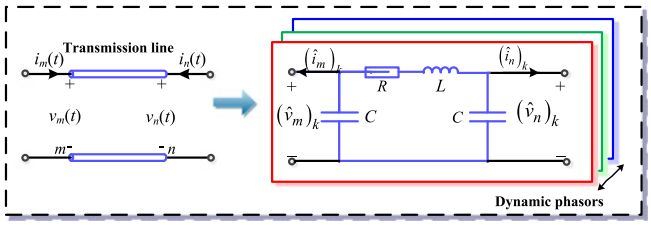

Fig. 1. Dynamic phasor based interface model (DPIM).

According to (1)–(2), the corresponding dynamic phasor model of (3) can be derived

$$\begin{cases} \frac{d\widehat{\boldsymbol{x}}_{\boldsymbol{k}}(t)}{dt} = A_k\widehat{\boldsymbol{x}}_{\boldsymbol{k}}(t) + B\widehat{\boldsymbol{v}}_{\boldsymbol{k}}(t), \\ \widehat{\boldsymbol{i}}_{\boldsymbol{k}}(t) = C\widehat{\boldsymbol{x}}_{\boldsymbol{k}}(t) + D\widehat{\boldsymbol{v}}_{\boldsymbol{k}}(t), \end{cases} \tag{4}$$

where $A_k = A - jk\omega I$.

For simplicity, time variable t is omitted hereafter. And (4) is rewritten in the real and imaginary part separately as

$$\frac{d}{dt}\begin{bmatrix} \widehat{\boldsymbol{x}}_{\boldsymbol{R,k}} \\ \widehat{\boldsymbol{x}}_{\boldsymbol{I,k}} \end{bmatrix} = \begin{bmatrix} A & k\omega I \\ -k\omega I & A \end{bmatrix}\begin{bmatrix} \widehat{\boldsymbol{x}}_{\boldsymbol{R,k}} \\ \widehat{\boldsymbol{x}}_{\boldsymbol{I,k}} \end{bmatrix} + B\begin{bmatrix} \widehat{\boldsymbol{v}}_{\boldsymbol{R,k}} \\ \widehat{\boldsymbol{v}}_{\boldsymbol{I,k}} \end{bmatrix}, \text{ and} \tag{5}$$

$$\begin{bmatrix} \widehat{\boldsymbol{i}}_{\boldsymbol{R,k}} \\ \widehat{\boldsymbol{i}}_{\boldsymbol{I,k}} \end{bmatrix} = C\begin{bmatrix} \widehat{\boldsymbol{x}}_{\boldsymbol{R,k}} \\ \widehat{\boldsymbol{x}}_{\boldsymbol{I,k}} \end{bmatrix} + D\begin{bmatrix} \widehat{\boldsymbol{v}}_{\boldsymbol{R,k}} \\ \widehat{\boldsymbol{v}}_{\boldsymbol{I,k}} \end{bmatrix}, \tag{6}$$

where $\widehat{\boldsymbol{x}}_{\boldsymbol{R,k}} = Re(\widehat{\boldsymbol{x}}_{\boldsymbol{k}})$, $\widehat{\boldsymbol{x}}_{\boldsymbol{I,k}} = Im(\widehat{\boldsymbol{x}}_{\boldsymbol{k}})$, $\widehat{\boldsymbol{v}}_{\boldsymbol{R,k}}$, $\widehat{\boldsymbol{v}}_{\boldsymbol{I,k}}$, $\widehat{\boldsymbol{i}}_{\boldsymbol{R,k}}$, $\widehat{\boldsymbol{i}}_{\boldsymbol{I,k}}$ are the real and imaginary part of the voltage and the current, respectively.

The k^{th} dynamic phasors of voltage and current are calculated after solving (5) as follows

$$\begin{cases} \widehat{\boldsymbol{v}}_{\boldsymbol{k}} = \widehat{\boldsymbol{v}}_{\boldsymbol{R,k}} + j\widehat{\boldsymbol{v}}_{\boldsymbol{I,k}}, \\ \widehat{\boldsymbol{i}}_{\boldsymbol{k}} = \widehat{\boldsymbol{i}}_{\boldsymbol{R,k}} + j\widehat{\boldsymbol{i}}_{\boldsymbol{I,k}}. \end{cases} \tag{7}$$

B. Dynamic Phasor Based Interface Models

In previous studies, the dynamic phasor technique is widely used for the quasi steady state model of power electronic devices to improve the simulation efficiency [16]–[19], but has not been applied for hybrid simulations. As the technique derived by dynamic phasors can not only provide the instantaneous values, but also steady-state phasor values, it is more suitable to derive the interface model for hybrid simulations.

Generally, in the simulation of TS subsystems, the frequency concerned equals to or less than 50 Hz [5]. Moreover, all the transmission lines in the TS subsystem are modeled by the lump parameter circuits, i.e., PI circuit model [8]. Therefore, the impact from the TS subsystem on the EMT subsystems will include only the electro-mechanical dynamics, and the PI-section model is accurate enough to capture the interested electro-mechanical dynamics. Correspondingly, the interface line, represented by the PI-section model, is derived by dynamic phasors and named as the DPIM (see Fig. 1). The DPIM is implemented as a customer-defined module in the EMT program that calculates parameters of interfaces. The derivation of the DPIM is given as follows.

First, the corresponding differential equation of interface line from node m to node n is given as

$$\begin{cases} (\widehat{u}_m)_k = (\widehat{i}_{mn})_k[R + (p + j\omega)L] + (\widehat{u}_n)_k, \\ (p + j\omega)C(\widehat{u}_m)_k = (\widehat{i}_m)_k - (\widehat{i}_{m,n})_k, \\ (p + j\omega)C(\widehat{u}_n)_k = (\widehat{i}_n)_k + (\widehat{i}_{m,n})_k, \end{cases} \tag{8}$$

where R, L are the line resistance and inductance; C is the capacitor value; $p = d/d(t\omega_B)$; ω_B is the base value of angular velocity; $(\widehat{u}_m)_k$, $(\widehat{u}_n)_k$ are the k^{th} dynamic phasors of voltages of node m and n; $(\widehat{i}_{m,n})_k$ is the k^{th} dynamic phasors of the branch current.

After rewriting, (8) is transformed as

$$\begin{cases} \frac{d(\widehat{i}_{mn})_{R,k}}{dt} = \omega_B \frac{-R(\widehat{i}_{mn})_{R,k} + X(\widehat{i}_{mn})_{I,k} + (\widehat{u}_m)_{R,k} - (\widehat{u}_n)_{R,k}}{L}, \\ \frac{d(\widehat{i}_{mn})_{I,k}}{dt} = \omega_B \frac{-R((\widehat{i}_{mn})_{I,k} - X(\widehat{i}_{mn})_{R,k} + (\widehat{u}_m)_{I,k} - ((\widehat{u}_n)_{I,k}}{L}, \\ \frac{d(\widehat{u}_m)_{R,k}}{dt} = \omega_B \frac{X_C(\widehat{u}_m)_{I,k} + (\widehat{i}_m)_{R,k} - (\widehat{i}_{mn})_{R,k}}{C}, \\ \frac{d(\widehat{u}_m)_{I,k}}{dt} = \omega_B \frac{-X_C(\widehat{u}_m)_{R,k} + (\widehat{i}_m)_{I,k} - (\widehat{i}_{mn})_{I,k}}{C}, \\ \frac{d(\widehat{u}_n)_{R,k}}{dt} = \omega_B \frac{X_C(\widehat{u}_n)_{I,k} + (\widehat{i}_n)_{R,k} + (\widehat{i}_{mn})_{R,k}}{C}, \\ \frac{d(\widehat{u}_n)_{I,k}}{dt} = \omega_B \frac{-X_C(\widehat{u}_n)_{R,k} + (\widehat{i}_n)_{I,k} - (\widehat{i}_{mn})_{I,k}}{C}, \end{cases} \tag{9}$$

where X_C is the capacitance; the subscripts R, I denote the real and imaginary parts of dynamic phasors. (9) is the corresponding state-space equation of DPIM. In particular, when $k = 1$, (9) gives the positive-sequence dynamic phasor model. This model can provide instantaneous interface variables but also fundamental frequency values of the positive sequence. Similarly, when $k = -1$, values in the negative sequence can also be derived.

C. Comparisons With Traditional Interface Model

The specific computational step of calculating parameters of interfaces is compared between the proposed DPIM and the DFT/FFT technique. For hybrid simulations, the FFT/DFT technique is generally used to extract fundamental values of EMT subsystems [12]. Taking use of the symmetry and periodicity of DFT coefficients, the FFT technique is more efficient than the DFT technique, but their principles are the same [20]. Taking the interface current $i(k)$ as an example, its corresponding DFT expression is given as

$$\begin{cases} I(k) = \sum_{n=0}^{N-1} i(n) e^{-j\frac{2\pi}{N}nk}, \\ i(k) = \frac{1}{N}\sum_{n=0}^{N-1} I(k) e^{j\frac{2\pi}{N}nk}, \end{cases} \tag{10}$$

where N is the number of samples during a sampling cycle. According to the reference [20], the computational complexity of FFT is in the order of $O_{\mathrm{FFT}} = O(Nlog_2N)$. For the proposed DPIM, if (9) is derived by the Trapezoidal algorithm, two additions and four multiplications are required for calculations of each differential equation. And thus the computational complexity is $O_{DP} = O(Ck)$, $k \leq 3$ where k is the maximum order of dynamic phasors and C is constant less than 50. As k is much smaller than N (N is normally more than $f_s/f = 400$, where f_s is sampling frequency, which equals 2000 Hz in our case, f is system frequency, which equals 50 Hz in our case). Obviously, the computation complexity of the proposed DPIM is much smaller than that of the FFT technique. This is one reason why the proposed DPIM is more efficient than the FFT technique. On the other aspect, as the interface circuit is modeled by DPIM, the nodal conductance matrix of the EMT subsystem can be reduced slightly, and the overall simulation efficiency will be further improved.

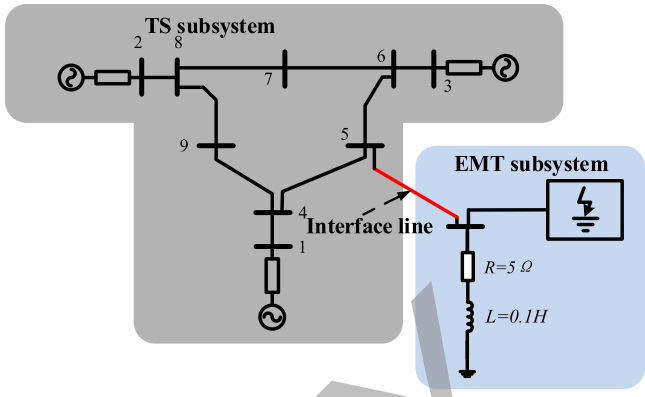

Fig. 2. IEEE 9 system with the constant R-L load.

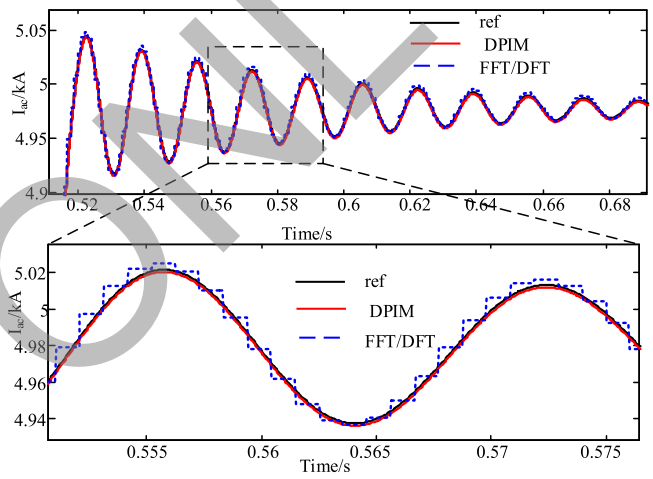

Fig. 3. Comparisons of interface currents under different methods.

For better illustration, the IEEE 9-bus system with the constant R-L load (see Fig. 2) is used for the case studies to demonstrate the advantages of DPIM in accuracy improvement over the DFT/FFT technique. As shown in Fig. 2 , the IEEE 9-bus system is located in the TS subsystem, while the constant R-L load is placed in the EMT subsystem. They are connected through an interface line. One of the tested cases is to trigger a three-phase fault on the bus feeding the load at $t = 0.5$ s. The fault lasts for 200 ms and then disappears. The transient responses are obtained by the hybrid simulations with both the DPIM and the FFT/DFT techniques. The time steps of TS/EMT subsystems are 5 ms/20 μs, respectively. For comparison, the references results are obtained by only using the EMT simulation with a time step of 20 μs. All results are displayed in Fig. 3.

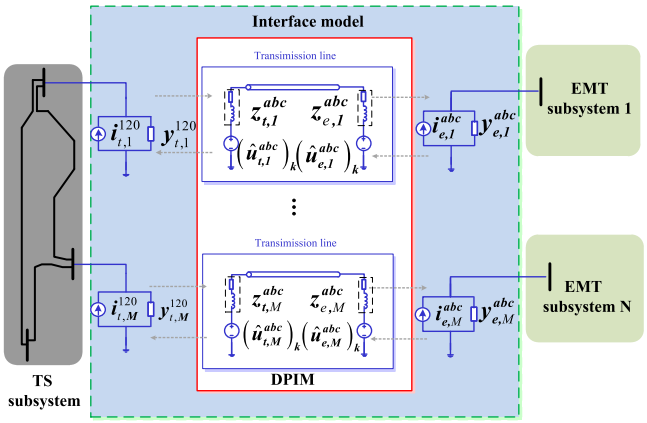

Fig. 4. Interface models between DPIM and EMT/TS subsystems.

It can be seen that the results of DPIM are more accurate than those of the FFT/DFT technique. Moreover, the latter suffers from the errors induced by the sampling delays. As a discrete method, the FFT/DFT technique has the simulation output remain constant during the sampling intervals (1 ms). As a result, significant errors are caused by the FFT/DFT technique in the EMT subsystem when the time step is 20 μs. Therefore, the proposed DPIM can improve the accuracy of the interface values. And thus the accuracy of the overall simulation is greatly enhanced.

III. Hybrid EMT-TS Simulation

A. Hybrid Simulation Using DPIM

As shown in Fig. 4, the hybrid simulation starts with the separation of the whole AC/DC systems into EMT and TS subsystems, where the interface lines are represented with the DPIM. The DPIM and EMT subsystems are simulated under the same EMT program, where DPIM is implemented by the customer-defined module. The TS subsystem is simulated under the TS program. Among the three parts, the most detailed part covering the widest frequency range is the EMT subsystem. The frequency range is determined by the time step [21]. If a time step of 50 μs is used, the maximum theoretical frequency will reach 20 kHz, but only up to 10 kHz can be reproduced accurately according to the Nyquist criterion. The second detailed part is DPIM, where the frequency range is determined by the order of dynamic phasors.

Here the interfaces of the proposed hybrid simulation method have two parts. The first part is the interface between EMT subsystem and DPIM, where the impact of EMT subsystem on DPIM is represented by Thevenin equivalents (dynamic phasor form), and the impact of DPIM on EMT subsystem is represented by Norton equivalents (three-phase instantaneous form). During each iteration, the dynamic phasors of interface currents in the DPIM are converted into three-phase instantaneous form, the Norton equivalents in the EMT subsystem are then derived. Similarly, the Thevenin voltages are calculated and transformed into the dynamic phasor forms, then the Thevenin equivalents in the DPIM are derived correspondingly. The second part is the interface between DPIM and the TS subsystem. The three sequence interface voltages in the TS subsystem are converted into the dynamic phasor form, constituting the impact of TS subsystem onto the DPIM. Then dynamic phasors of interface currents are calculated by DPIM. These currents are transformed into the corresponding three-sequence Norton equivalent currents, constituting the impact of DPIM onto the TS subsystem. The parameters of interfaces between DPIM and TS subsystem are delivered via LAN (e.g., TCP/UDP socket server [17]).

The interface models between EMT/TS subsystem and DPIM will be elaborated in Section B and C, respectively. The general simulation procedure will be given in Section D.

B. Interface Model Between EMT Subsystem and DPIM

The impacts of EMT subsystem on DPIM are presented by Thevenin equivalents (dynamic phasor form), i.e. Thevenin voltage $(\hat{u}_e^{\mathrm{abc}})_k(t_m),\ k=0,\pm1,\pm2...\pm K$ and Thevenin impedance $z_e^{\mathrm{abc}}(t_m)$ in Fig. 4, where K is the order of dynamic phasors; t_m is the m_{th} simulation step of the TS subsystem. For simplicity, the interface index will be omitted hereinafter if not specially mentioned.

Here, Thevenin voltages $(\hat{u}_e^{\mathrm{abc}})_k(t_m),\ k=0,\pm1,\pm2...\pm K$ are calculated in DPIM based on (9). The Thevenin impedance $z_e^{\mathrm{abc}}(t_m)$ is given by

$$z_e^{\mathrm{abc}}(t_m) = R_e^{\mathrm{abc}}(t_m) + j\omega L_e^{\mathrm{abc}}(t_m), \tag{11}$$

where $R_e^{\mathrm{abc}}(t_m), L_e^{\mathrm{abc}}(t_m)$ are the three-phase resistance and inductance matrices at time t_m. They can be derived at the beginning of the simulations.

The impact of DPIM on EMT subsystem is represented by Norton equivalents (three-phase instantaneous form), i.e. Norton current $i_e^{\mathrm{abc}}(t_m)$ and equivalent conductance $y_e^{\mathrm{abc}}(t_m)$ in Fig. 4. Based on (9), dynamic phasors of interface current in the EMT subsystem $(\hat{i}_e^{\mathrm{abc}})_k(t_m),\ k=0,\pm1,\pm2...\pm K$ are calculated, and then the Norton equivalent current in the instantaneous values are derived as

$$i_e^{\mathrm{abc}}(t_m) = \sum_{k=0}^{K} (\hat{i}_e^{\mathrm{abc}})_k(t_m) e^{jk\omega t_m}. \tag{12}$$

Similarly, the Norton admittance, $y^{\mathrm{abc}}(t_m)$ can be obtained from the admittance matrix of each EMT subsystem as

$$y_e^{\mathrm{abc}}(t_m) = [R_{dp}^{\mathrm{abc}}(t_m) + j\omega L_{dp}^{\mathrm{abc}}(t_m)]^{-1}, \tag{13}$$

where $R_{dp}^{\mathrm{abc}}(t_m),\ L_{dp}^{\mathrm{abc}}(t_m)$ are the corresponding DPIM three-phase resistance and inductance matrix at time t_m.

C. Interface Model Between DPIM and TS Subsystem

For DPIM, the impact of TS subsystem is represented by Thevenin equivalents (dynamic phasor form), i.e. Thevenin voltage$(\hat{u}_t^{\mathrm{abc}})_k(t_m),\ k=0,\pm1,\pm2...\pm K$ and Thevenin impedance $z_t^{\mathrm{abc}}(t_m)$ in Fig. 4 [11]. As the positive, negative and zero sequence components at the fundamental frequency are considered in the TS subsystem, the order of dynamic phasors $(\hat{u}_t^{\mathrm{abc}})_k(t_m), k=0,\pm1$ correspond to the Thevein voltages in the zero, positive and negative sequence, respectively.

The calculations of equivalent impedance $z_t^{\mathrm{abc}}(t_m)$ is similar to that of the interface between EMT subsystem and DPIM.

For the TS subsystem, the interface is represented by its Norton equivalents, i.e., Norton equivalent current $i_t^{120}(t_m)$ as well as the equivalent admittance $y_t^{120}(t_m)$. First, the dynamic phasors of DPIM are derived based on (9). Then, interface voltages and currents of the fundamental frequency are derived by

$$\begin{cases} u^{\mathrm{abc}}(t_m) = 2(\hat{u}^{\mathrm{abc}})_{R,1}(t_m), \\ i^{\mathrm{abc}}(t_m) = 2(\hat{i}^{\mathrm{abc}})_{R,1}(t_m). \end{cases} \tag{14}$$

where $\hat{u}_{R,1}^{\mathrm{abc}}(t_m)$, $\hat{i}_{R,1}^{\mathrm{abc}}(t_m)$ are the real part of the first order dynamic phasors.

Interface voltages and currents in the three sequence domain $u^{120}(t_m)$, $i^{120}(t_m)$ are calculated based on the abc-120 transformation. Finally, the Norton equivalent current $i_t^{120}(t_m)$ is calculated by

$$i_t^{120}(t_m) = i^{120}(t_m) + y^{120}(t_m)u^{120}(t_m). \tag{15}$$

Similarly, the equivalent admittance, $y_t^{120}(t_m)$ can be obtained from the admittance matrix of each EMT subsystem, or

$$y_t^{120}(t_m) = [R_t^{120}(t_m) + j\omega L_t^{120}(t_m)]^{-1}, \tag{16}$$

where $R_t^{120}(t_m)$, $L_t^{120}(t_m)$ are the three-sequence resistance and inductance matrices at time t_m.

D. Computational Scheme

The overall computational scheme of the proposed method, is illustrated in Fig. 5. It has the following steps:

first, the system is partitioned into the EMT subsystem, TS subsystem and the DPIM after the power-flow initialization. Then, the EMT subsystem will be simulated with an identical smaller step h (usually 10–100 μs), while the TS subsystem is simulated with a much larger step h_{ts}. The rate ratio is defined as $n = h_{ts}/h$. The choice of the rate ratio is dependent upon the requirement of simulation accuracy and numerical stability [21], [22]. Next, different subsystems are simulated in a distributed and coordinated way. First, the TS subsystem is simulated by the TS program. And then, interface parameters are transferred from the TS subsystem to the DPIM, where the interface variables are converted from the three-sequence form to the dynamic phasor form. Next, the intefaces between DPIM and EMT subsystem are updated. Both DPIM and EMT subsystems are calculated in the same EMT program, such as PSCAD/EMTDC, where DPIM is implemented as a customer-defined module.

DPIM and the EMT subsystem are simulated in parallel n times to fulfil the simulations within a whole time step h_{ts}. After that, parameters of the Norton equivalents in the TS subsystem are updated based on (14)–(15). Then the TS subsystem is simulated for the same time step h_{ts}. Finally, when the total time ($T_{\max}$) is reached, the simulation comes to an end and the results are output.

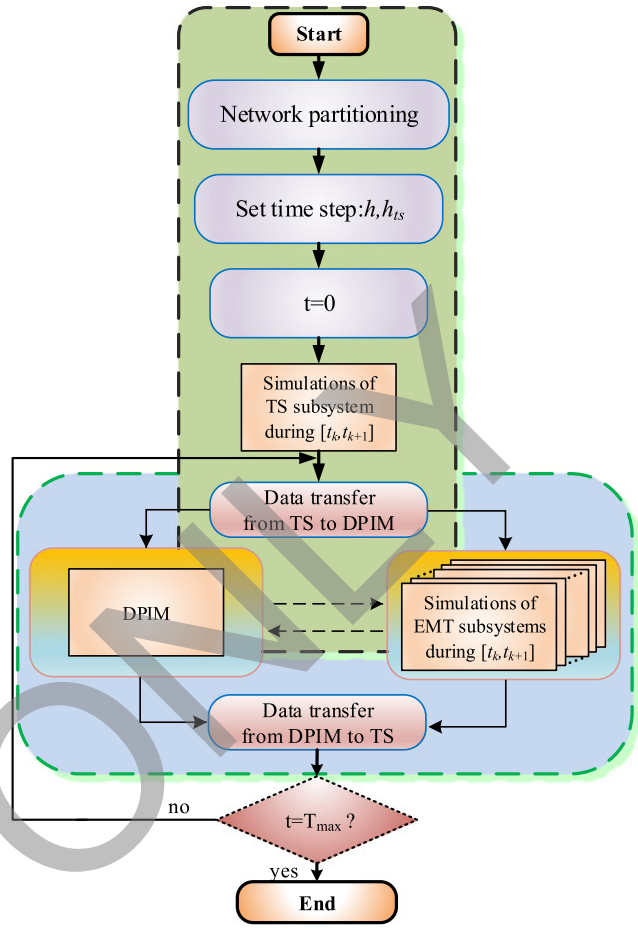

Fig. 5. Calculation procedure of the proposed method.

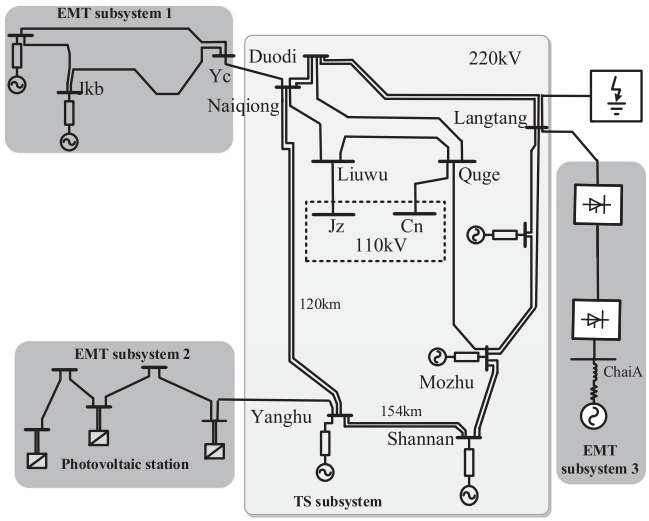

Fig. 6. Studied system.

IV. Case Studies

To evaluate the accuracy and efficiency of the proposed hybrid method as well as to compare it with the traditional one [9], [10], case studies are carried out on a practical HVDC project, where the Qinghai-Tibet HVDC is connected to a weak AC system (ESCR = 2.45), as shown in Fig. 6. The parameters of the 12-pulse two terminal HVDC is given as follows: the rated DC power is 800 MW; the rated DC voltage is 400 kV; the rated DC current is 1 kA, and the length of the DC cable is 120 km. The 110 kV and 220 kV buses of the main AC grids are shown

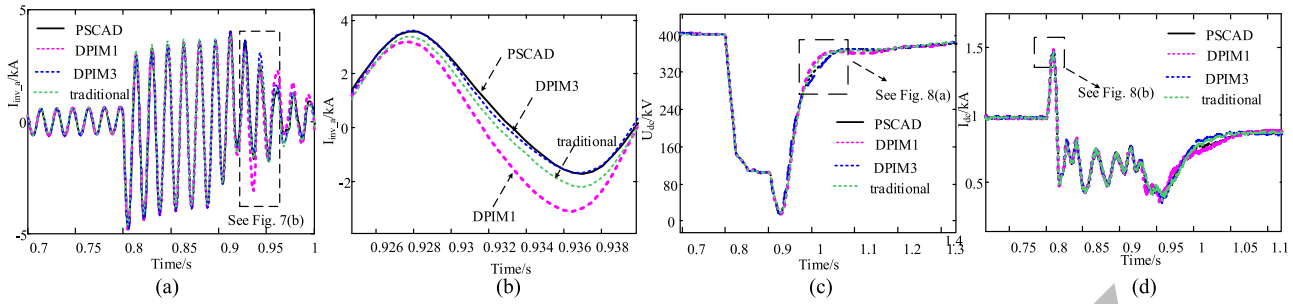

Fig. 7. Curves of the DPIM with different orders in comparison with the traditional method: (a) ac current of the inverter; (b) enlarged curves of a; (c) DC voltage; (d) DC current.

in Fig. 6, where system parameters are referred to [22]. The power transmission direction is from ChaiA (rectifier) station to Langtang (inverter) station. In the proposed method, areas with detailed dynamics are located in the EMT subsystems. For example, the HVDC associated with its control and protection system are assigned in the EMT subsystem 3. The simulation time of TS/EMT subsystem are 5 ms/20 μs, respectively. As the interface variables at the fundamental frequency are transmitted from the EMT subsystem to the TS subsystem, the dynamic phasors in this paper reserves to the third order. In the simulation results, DPIM1/DPIM3 refers to results obtained by dynamic phasors of order 1/3; method in [10] is marked as traditional; the reference results are obtained by simulating the whole system using the PSCAD/EMTDC with an unanimous time step of 20 μs.

Simulation results will be compared and a metric called the relative average simulation error is defined to quantify the simulation accuracy

$$\epsilon_{\text{avg}} = \frac{1}{N}\sum_{i=1}^{N} ||x_{\text{num},i} - x_{\text{ref},i}||/||x_{\text{ref},i}||, \qquad (17)$$

where $x_{\text{num},i}$, $x_{\text{ref},i}$ are the i_{th} sample of monitored variable x in per unit that are produced by different methods; N is the number of samples.

A. *Three-Phase Fault at Inverter-Side AC Bus*

In this scenario, a symmetric fault is appied at the AC bus of Langtang Station, where the three-phase inductive fault at phase A starts at $t = 0.8$ s. The grounding inductor is 0.1 H and the fault lasts 100 ms. Results of DPIM1/DPIM3 and the traditional method are shown in Fig. 7. As can be seen, results of DPIM3 overlaps with the reference, while those of DPIM1 and the traditional method have obvious errors. As can be observed from Fig. 7(b), through the method of DPIM3, the accuracy of the fault currents are obviously improved in transient circumstances compared to the traditional method. The recovery process of DC voltage and the zoomed-in curves of the DC current are shown in Fig. 8. From Fig. 8(a), the recovery time of U_{dc} for both the DPIM3 and the reference curve takes 0.14 s, while that of the traditional model takes 0.09 s, which has obvious errors. The differences between DPIM3 and the traditional one is because errors induced by the sampling delays of the traditional method

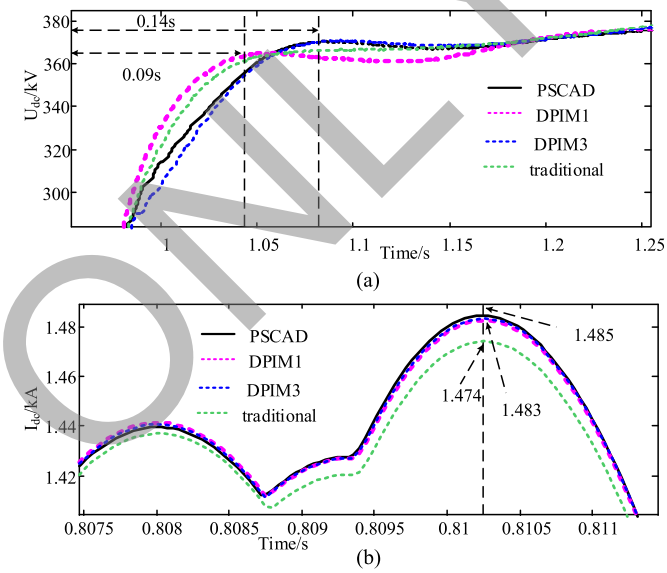

Fig. 8. Zoomed-in curves of DC voltage and DC current.

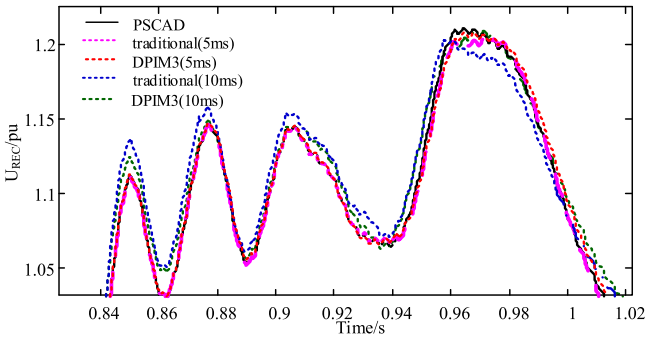

Fig. 9. Curves of the DPIM and the traditional method with different interaction time step lengths.

is larger than those of the DPIM3, resulting in the changes of damping of the system and affecting the recovery process of the DC voltage. As is shown in Fig. 8(b) of the zoomed-in curve of the DC current, the peak value of DPIM3 is closer to the reference value, reducing the errors from 0.011 pu to 0.002 pu.

According to Figs. 7 and 8, the appropriate order of DPIM for the proposed method is reserved to be three. The reason is given as follows: the three-phase balance is generally guaranteed

TABLE I
COMPARISON OF AVERAGE SIMULATION ERRORS (UNIT: IN PU) UNDER DIFFERENT INTERACTIVE TIME STEPS (THREE-PHASE FAULT SCENARIO

Method	DPIM1			DPIM3			TRA		
interactive time step/μs	2 ms	5 ms	10 ms	2 ms	5 ms	10 ms	2 ms	5 ms	10 ms
U_{dc}	0.0251	0.0527	0.0949	0.0030	0.0064	0.0452	0.0500	0.0784	0.1531
I_{dc}	0.0081	0.0179	0.0498	0.0020	0.0034	0.0217	0.0200	0.0399	0.0807
P_{inv}	0.0297	0.0505	0.0750	0.0050	0.0077	0.0300	0.0400	0.0760	0.1412
$V_{\mathrm{inv-a}}$	0.0050	0.0064	0.0248	0.0010	0.0017	0.0155	0.0100	0.0211	0.0443
$I_{\mathrm{inv-a}}$	0.0400	0.0711	0.1041	0.0080	0.0111	0.0496	0.0500	0.1070	0.2077

in selecting the interfaces between TS and EMT subsystems. This makes the interface variables mostly of the fundamental frequency. Harmonic components only appear in faulty conditions, especially following an asymmetric fault. Even so, the interface variables have very small harmonics higher than the order of 3 because of the DC filters. Therefore, in our special cases of LCC-HVDC system, the appropriate order of DPIM is 3. Those higher (than 3) -order phasors of the DPIM are ignored, which will not affect the accuracy of the simulation.

Fig. 9 shows the rectifier voltages of DPIM3 and the traditional one under different interactive time step ($= h_{ts}$). As can be seen, with the increase of the interactive time step, errors of both DPIM3 and the traditional one are increased, but the errors of DPIM3 increase more slowly. Relative average simulation errors of different methods are given in Table I. As can be seen, errors of DPIM3 are the smallest. DPIM3 has obvious improvement in accuracy over the traditional method concerning the DC quantities. When the interactive time step equals to 5 ms, errors of DC voltages are reduced from 0.078 pu to 0.006 pu, reaching an 12 times improvement of accuracy. According to the analysis in Section II(C), the reason why DPIM3 will achieve higher simulation precision over the traditional method is that the interface variables of the current time are obtained and errors induced by sampling delays are reduced. As the interactive time step increases, the advantages of the proposed method over the traditional one will be more obvious, which is also shown in Table I.

Fig. 10 shows the positive and negative sequence component associated with their dynamic phasors. As is shown, $2(\hat{i}_e^{\mathrm{abc}})_{R,1}(t_m)$, $2(\hat{i}_e^{\mathrm{abc}})_{I,1}(t_m)$ are the envelopes of the positive and negative sequence component of the interface currents, respectively. Therefore, the first-order dynamic phasor $2(\hat{i}_e^{\mathrm{abc}})_{R,1}(t_m)$, $2(\hat{i}_e^{\mathrm{abc}})_{I,1}(t_m)$ can effectively represent the fundamental component of interface currents.

B. Single-Phase Fault at Inverter AC Bus

In this scenario, an asymmetric fault is appied at the AC bus of Langtang Station, where the single-phase inductive fault at phase A starts at $t = 0.8$ s. The grounding inductor is 0.1 H and the fault lasts 100 ms. Results of the proposed method and the traditional one are given in Fig. 11. As is shown, even in the asymmetric fault, results of DPIM3 are more accurate than those of the traditional one. From Fig. 11(c) and (d), the recovery processes of DC voltage and current are more accurate than those of DPIM1 and the traditional method. The improvement

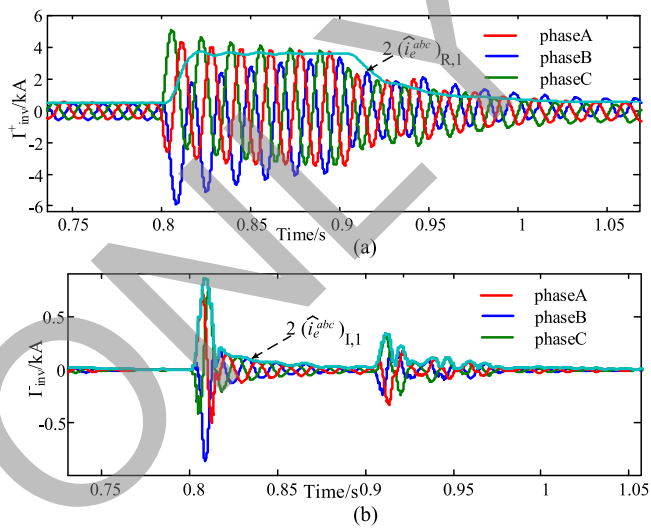

Fig. 10. Interface currents and its dynamic phasors.

of DPIM3 compared with DPIM1 is because during asymmetric faults, both second and third harmonic components of interfaces are calculated for DPIM3 while those of DPIM1 are neglected. The reason why DPIM3 has higher precision than the traditional method is sampling delay errors can be reduced by the proposed DPIM3. And these errors will lead to more obvious decrease of accuracy during asymmetric faults than symmetric faults.

Similarly, the inverter voltages of DPIM3 and the traditional one under different interactive time step ($= h_{ts}$) are shown in Fig. 12. As the interactive time step increases, the errors of DPIM3 increases more slowly compared with results of the traditional one. The positive and negative sequence component associated with their dynamic phasors are given in Fig. 13. As is shown, the first-order dynamic phasors $2(\hat{i}_e^{\mathrm{abc}})_{R,1}(t_m)$, $2(\hat{i}_e^{\mathrm{abc}})_{I,1}(t_m)$ are the envelopes of the positive and negative components of the interface currents. Therefore, in the case of the asymmetric fault, the dynamic phasors can effectively represent the fundamental frequency components of the interface current as well. Both these two scenarios have demonstrated that the advantage of the DPIM over the traditional interface model. That is to say, the proposed DPIM can provide the intantaneous and phasor values of interfaces simultaneously.

To quantify differences in accuracy under different interactive time steps, relative average simulation errors are given in

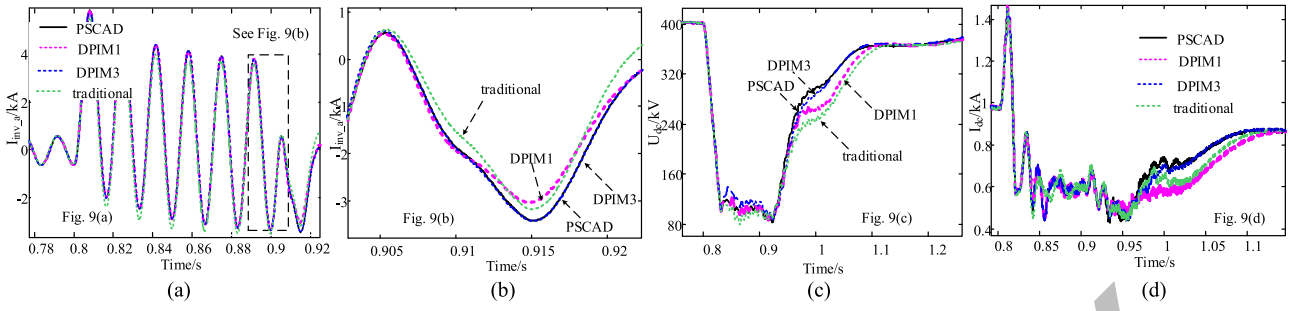

Fig. 11. Curves of the DPIM with different orders and the traditional method: (a) ac current of the inverter; (b) enlarged curves of a; (c) DC voltage; (d) DC current.

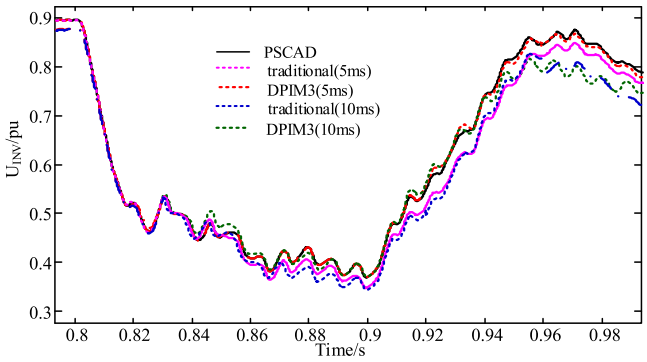

Fig. 12. Zoomed-in curves of DC current.

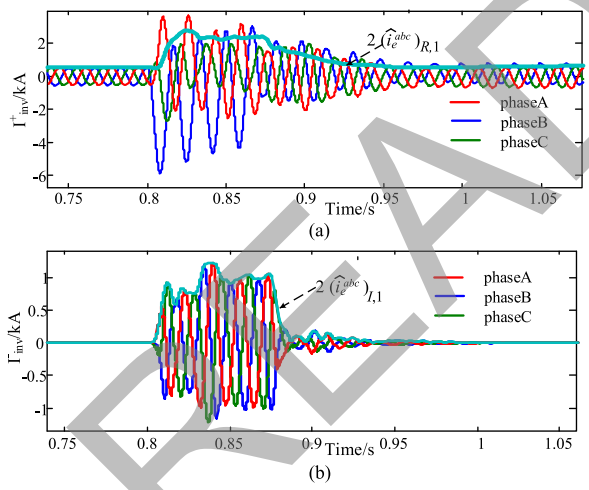

Fig. 13. Interface currents and its dynamic phasors.

Table II. And the errors of DPIM3 is the smallest, the improving in simulation accuracy is even more obvious than results during the three-phase symmetric fault. When the interactive time step is 5 ms, errors of the DC power are reduced from 0.255 pu to 0.071 pu. Compared with results during the three-phase symmetric fault, errors aroused by sampling delays is more obvious during the asymmetric fault. Therefore, the proposed method has more obvious advantages in the scenarios of asymmetric faults than the traditional method.

C. Analyses on Factors Affecting the Accuracy of Interfaces

As demonstrated, the primary purpose of the DPIM is to improve the accuracy of interfaces. Many factors affect the accuracy of interfaces, such as, interaction time steps, the time-step of the TS subsystem and interface line length, etc. It should be noted that the accuracy of interface AC currents is more sensitive to the parameters of interfaces. From Fig. 14, it is shown that even though errors of all the methods increase as the time-step of TS subsystem (h_{TS}) rises, the DPIM3 method is the most accurate, and it can achieve a 3 times improvement of accuracy than the traditional method. The relationship between ϵ_{avg} versus the length of interface line is given in Fig. 15. Specifically, when the length of interface line is shorter than 100 km, errors of the interface current by the traditional method is around 0.5 pu while the DPIM3 results have achieved almost 4 times improvement of accuracy. The errors of the traditional method will be largest when the length of the interface line is around 120 km. However, errors of the interface current by the DPIM3 is below 0.2 pu. Errors of all the methods will drop gradually and the error gap between the proposed method and the traditional method will gradually drop when the length of the interface is further increased. This is because when the length of the interface increases to more than 200 km, the fast electromagnetic transients will gradually disappear when they spread from the EMT subsystem to the TS subsystem and only components of fundamental frequency exist around the interfaces.

D. Comparisons of Computational Performance

The total CPU time and the time consumed by updates of interfaces are compared in Fig. 16, where the simulation period for the case is 3 s. It is shown that the proposed method is more efficient than the traditional method. The simulation time is reduced from 576 s to 342 s, 23 times faster than the full EMT methods and achieving an improvement of 68.2% compared with the traditional method. It is because that the proposed method has better efficiency in calculations of interfaces and interactive process than the traditional one. Considering its previously demonstrated advantages in simulation accuracy, the proposed method is more suitable for the simulations of large-scale AC/DC systems.

TABLE II
COMPARISON OF AVERAGE SIMULATION ERRORS (UNIT: IN PU) UNDER DIFFERENT INTERACTIVE TIME STEPS (SINGLE-PHASE FAULT SCENARIO)

Method	DPIM1			DPIM3			TRA		
Interactive Time step/μs	2 ms	5 ms	10 ms	2 ms	5 ms	10 ms	2 ms	5 ms	10 ms
U_{dc}	0.0586	0.1113	0.3896	0.0120	0.0405	0.0856	0.0900	0.1970	0.2904
I_{dc}	0.0130	0.0272	0.0626	0.0050	0.0115	0.0662	0.0300	0.0449	0.0921
P_{inv}	0.0782	0.1666	0.3547	0.0414	0.0700	0.2500	0.1207	0.2550	0.3224
$V_{\mathrm{inv-a}}$	0.0085	0.0127	0.0394	0.0030	0.0063	0.0359	0.0150	0.0222	0.0460
$I_{\mathrm{inv-a}}$	0.1117	0.2346	0.4927	0.0600	0.1072	0.3275	0.1700	0.3493	0.4357

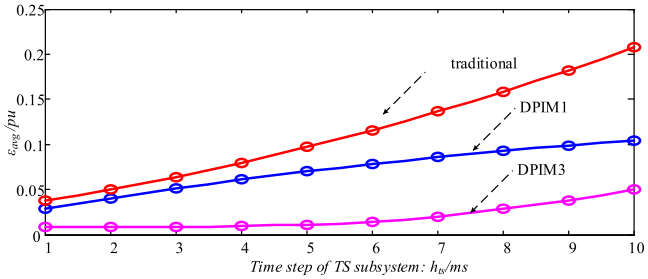

Fig. 14. Relationship between ϵ_{avg} versus the time step of TS subsystem (h_{TS}).

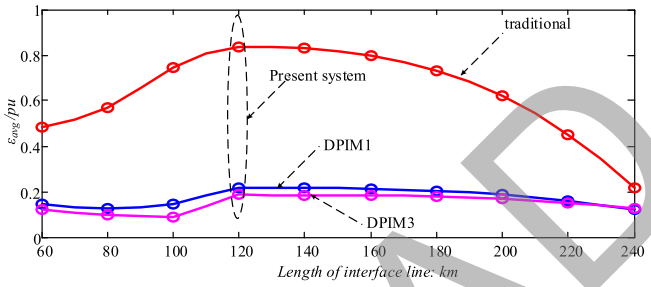

Fig. 15. Relationship between ϵ_{avg} versus the length of interface line (The parameters are: impedance $r_0 = 0.27\ \Omega$/km, inductance $l_0 = 13$ mH/km, capacitance $c_0 = 1.33\ \mu$F/km).

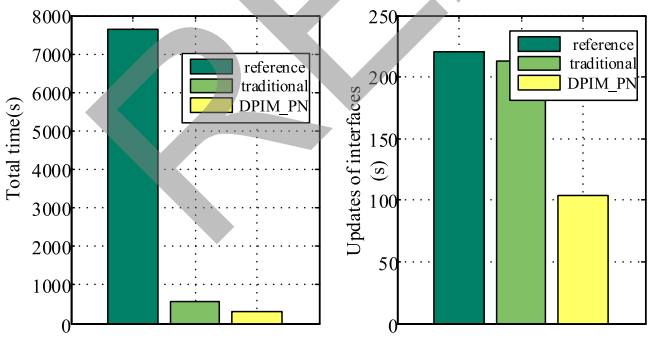

Fig. 16. Total time and time consumed by updates of interfaces.

V. CONCLUSION

In this paper, a novel dynamic phasor based interface model (DPIM) is proposed to improve the simulation accuracy of hybrid simulations, especially with the applications for transmission of large-scale renewable energy by LCC-HVDC. One of its salient features is the DPIM, which is derived by dynamic phasors, can improve the accuracy and reduce the computation of the interface model in the TS subsystem. The other important feature is that the interface model of the EMT subsystem, with its instantaneous values represented by dynamic phasors, can be efficiently updated with the proposed DPIM. Moreover, the errors caused by the sampling delays are effectively mitigated. The effectiveness of the proposed method has been validated by a practical HVDC project. The proposed method increases the simulation speed by 23 times than the full EMT results, and 68.2% faster than the traditional method. Moreover, the errors of the interface currents are reduced by 47.6%. The above results have demonstrated its advantages in simulating large-scale AC/DC systems.

REFERENCES

[1] J. M. Carrasco *et al.*, "Power electronic systems for the grid integration of renewable energy sources: A survey," *IEEE Trans. Power Electron.*, vol. 53, no. 4, pp. 1002–1016, Aug. 2006.
[2] L. Wang and M. S. N. Thi, "Stability enhancement of large-scale integration of wind, solar, and marine-current power generation fed to an SG-based power system through an LCC-HVDC link," *IEEE Trans. Sustain. Energy*, vol. 5, no. 1, pp. 160–170, Jan. 2014.
[3] R. Torres-Olguin, M. Molinas, and T. Undeland, "Offshore wind farm grid integration by VSC technology with LCC-based HVDC transmission," *IEEE Trans. Sustain. Energy*, vol. 3, no. 4, pp. 899–907, Oct. 2012.
[4] J. Cao and J. Y. Cai, "HVDC in China," presented at the *EPRI, 2013 HVDC FACTS Conf.*, Palo Alto, CA, USA, Aug. 2013.
[5] V. Jalili-Marandi, V. Dinavahi, K. Strunz, J. A. Martinez, and A. Ramirez, "Interfacing techniques for transient stability and electromagnetic transient programs," *IEEE Trans. Power Del.*, vol. 24, no. 4, pp. 2385–2395, Oct. 2009.
[6] F. Plumier *et al.*, "Co-simulation of electromagnetic transients and phasor Models: A relaxation approach," *IEEE Trans. Power Del.*, vol. 31, no. 5, pp. 2360–2369, Oct. 2016.
[7] D. Shu *et al.*, "A novel interfacing technique for distributed hybrid simulations combining EMT and transient stability models,"*IEEE Trans. Power Del.*, to be published.
[8] X. Lin, A. M. Gole, and M. Yu, "A wide-band multi-port system equivalent for real-time digital power system simulators," *IEEE Trans. Power Syst.*, vol. 24, no. 1, pp. 237–249, Feb. 2009.
[9] Y. Liang, X. Lin, A. M. Gole, and M. Yu, "Improved coherency-based wide-band equivalents for real-time digital simulators," *IEEE Trans. Power Syst.*, vol. 26, no. 3, pp. 1410–1417, Aug. 2011.
[10] A. A. van der Meer *et al.*, "Combined simulation method for improved performance in grid integration studies including multi-terminal VSC-HVDC," in *Proc. IET Renew. Power Gener.*, Edinburgh, U.K., 2011, pp. 1–6.
[11] A. A. van der Meer, M. Gibescu, M. A. M. M. van der Meijden, W. L. Kling, and J. A. Ferreira, "Advanced hybrid transient stability and EMT simulation for VSC-HVDC systems," *IEEE Trans. Power Del.*, vol. 30, no. 3, pp. 1057–1066, Jun. 2015.

[12] Q. Huang and V. Vittal, "Application of electromagnetic transient-transient stability hybrid simulation to FIDVR study," *IEEE Trans. Power Syst.*, 2016, vol. 31, no. 4, pp. 2634–2646, Jul. 2016.
[13] C. Liu, A. Bose, and P. Tian, "Modeling and analysis of HVDC converter by three-phase dynamic phasor," *IEEE Trans. Power Del.*, vol. 29, no. 1, pp. 3–12, Feb. 2014.
[14] Y. Huang, M. Chapariha, F. Therrien, J. Jatskevich, and J. R. Mart, "A constant-parameter voltage-behind-reactance synchronous machine model based on shifted-frequency analysis," *IEEE Trans. Energy Convers.*, vol. 30, no. 2, pp. 761–771, Jun. 2015.
[15] M. Elizondo, F. Tuffner, and K. Schneider, "Simulation of inrush dynamics for unbalanced distribution systems using dynamic-phasor models," *IEEE Trans. Power Syst.*, vol. 32, no. 1, pp. 633–642, Jan. 2017.
[16] P. Mattavelli, A. M. Stankovic, and G. C. Verghese, "SSR analysis with dynamic phasor model of thyristor-controlled series capacitor," *IEEE Trans. Power Syst.*, vol. 14, no. 1, pp. 200–208, Feb. 1999.
[17] W. Stevens, *UNIX Network Programming, Vol. 1: Networking APIs: Sockets and XTI.* Englewood Cliffs, NJ, USA: Prentice-Hall, 1997.
[18] S. Chandrasekar and R. Gokaraju, "Dynamic phasor modeling of type 3 DFIG wind generators (including SSCI phenomenon) for short-circuit calculations," *IEEE Trans. Power Del.*, vol. 30, no. 2, pp. 887–897, Apr. 2015.
[19] M. Daryabak *et al.*, "Modeling of LCC-HVDC systems using dynamic phasors," *IEEE Trans. Power Del.*, vol. 29, no. 4, pp. 1989–1998, Aug. 2014.
[20] R. M. Corless and N. Fillion, *A Graduate Introduction to Numerical Methods*. New York, NY, USA: Springer, 2013.
[21] J. C. G. de Siqueira *et al.*, "A discussion about optimum time step size and maximum simulation time in EMTP-based programs," *Int. J. Electr. Power Energy Syst.*, vol. 72, pp. 24–32, 2015.
[22] D. Shu *et al.*, "Hybrid method for numerical oscillation suppression based on rational-fraction approximations to exponential functions," *IET Gener., Transm. Distrib.*, vol. 10, no. 11, pp. 2825–2832, Aug. 2016.

Dewu Shu (S'14) received the B.Sc. degree in electrical engineering from Tsinghua University, Beijing, China, in 2013, where he is currently working toward the Ph.D. degree in the Department of Electrical Engineering. His research interests include multi-rate EMT/TS simulations, and parallel and distributed computing.

Xiaorong Xie (SM'14) received the B.Sc. degree from Shanghai Jiao Tong University, Shanghai, China, in 1996, and the Ph.D./M.Eng. degrees from Tsinghua University, Beijing, China, in 2001. From 2001 to 2005, he was a Lecturer in the Department of Electrical Engineering, Tsinghua University, where has been working as an Associate Professor since 2005. His current research interests focus on power system analysis and control, and flexible ac transmission systems.

Venkata Dinavahi (SM'08) received the Ph.D. degree from the University of Toronto, Toronto, ON, Canada, in 2000. He is currently a Professor in the Department of Electrical and Computer Engineering, University of Alberta, Edmonton, AB, Canada. His research interests include real-time simulation of power systems and power electronic systems, large-scale system simulation, and parallel and distributed computing.

Chunpeng Zhang (M'10) received the B.S. and M.S. degrees from the Department of Electrical Engineering, Shandong University, Jinan, China, in 1997 and 2000, respectively. He is currently a Lecturer in the Department of Electrical Engineering, Tsinghua University, Beijing, China. His research interests include flexible ac transmission systems and power quality.

Xiaohui Ye received the B.Sc. degree from Tianjin University, Tianjin, China, in 2008, and the M.Sc. degree from Tsinghua Universitiy, Beijing, China, in 2010. In 2010, he joined the Power System Department of China Electrical Power Research Institute. Currently, he is working toward the Ph.D. degree in the Department of Electrical Engineering, Tsinghua University. His research interest are in the areas of power system simulation and analysis.

Qirong Jiang (M'98) received the B.S. and Ph.D. degrees in electrical engineering from Tsinghua University, Beijing, China, in 1992 and 1997, respectively. Since 2006, he has been a Professor with Tsinghua University. His research interests include power system analysis and control, modeling and control of flexible ac transmission systems, power quality analysis and mitigation, power-electronic equipment, and renewable energy power conversion.